Relativity and Structure in Neutron Stars

Brian Friesen

December 9, 2011

Abstract

We explore the structure of neutron stars using the Tolman-Oppenheimer-Volkoff equation of hydrostatic equilibrium, the solution to which describes the complete mechanical structure of a spherically symmetric, self-gravitating, static mass in general relativity. We close this equation by supplying a nuclear equation of state and calculate mass-radius and mass-central density relations, giving particular attention to the maximum mass predicted for a neutron star with this equation of state. Finally we compare these predictions to those from other work in the literature and discuss constraints imposed by neutron star masses inferred from observations.

1 Introduction

Neutron stars (NSs) are compact celestial objects which display some of the most exotic physical behavior of any objects in the observable universe. With mass densities of $\sim 5 \times 10^{15}$ g cm^{-3} and Fermi energies of $\sim$ 100 MeV, NS matter is more dense than nuclear matter, $\rho_{\text{nuc}} \sim 10^{14}$ g cm^{-3}, and even at the high temperatures characteristic of NSs ($10^6 - 10^8$ K), this enormous density renders much of it degenerate. At the macroscopic scale the matter produces gravitational fields so strong that general relativistic effects become substantial, rendering the Newtonian theory of gravity insufficient for predicting the physical properties of these stars.

This paper focuses primarily on the effects of general relativity on the structure of neutron stars, while also giving some attention to aspects of nuclear physics relevant in constructing the nuclear equation of state (EOS). Specifically we explore the structure of a simple neutron star model: a spherically symmetric, uncharged, non-rotating mass composed of a perfect (incompressible) fluid in general relativistic spacetime. This work is based on foundational calculations performed by Tolman 1939 and Oppenheimer and Volkoff 1939, but improves upon them by using more realistic EOSs as well as sophisticated numerical methods.

In Section 2 we review briefly the current NS observational efforts and results; next, in Section 3 we introduce the Tolman-Oppenheimer-Volkoff (TOV) differential equations and the properties of the spacetime from which they are constructed; in Section 4 we review properties of the EOS used to close this system of equations (this discussion is only cursory, given the complexity of nuclear theory); in Section 5 we discuss the role the TOV equations play in analyzing neutron star observations; Section 6 contains an overview of the numerical methods we have applied in solving these equations. Finally, in Section 7 we analyze our results and compare them both to other calculations existing in the literature, as well as to observations.

2 Neutron Star Observations

An NS forms when the core of a massive star ($\gtrsim 8M_\odot$) exhausts its nuclear fuel, with only iron "ash" remaining, and collapses under extreme gravitational pressure. During collapse the iron nuclei deleptonize via electron capture and eventually the density becomes so large that the short-range repulsive component of the strong force overwhelms that of gravity, causing the core to rebound and ejecting the outer layers of the star. This is a core-collapse supernova. What remains is a rapidly rotating mass of neutron-rich material with a strong magnetic field: a NS.

The angular velocity of NSs varies but can be as high as several 100 Hz; however rotation decelerates over time due to angular momentum loss from energy radiated away in their magnetic fields. Rapidly rotating NSs with misaligned magnetic and rotational axes emit intense beams of radio waves from their magnetic poles and appear to "pulse" as one pole sweeps across the Earth. These *pulsars* and were first discovered in 1967 (Hewish et al. 1968). However older NSs which have slowed significantly cease pulsating entirely (even though they are still rotating) and are much more difficult to detect (Chen and Ruderman 1993). So far only a handful have been discovered, the first in 1996 (Walter, Wolk, and Neuhäuser 1996). The difficulty in detecting these "plain" neutron stars stems from a combination of their blackbody-like nature and their small size. Such difficulty is evident through the following calculation. According to the Stefan-Boltzmann law the luminosity L of a blackbody with radius R and temperature T is

$$L = 4\pi R^2 \sigma T^4 \tag{1}$$

where $\sigma \simeq 5.67 \times 10^{-5}$ erg cm^{-2} s^{-1} K^{-4} is the Stefan-Boltzmann constant. Shortly after a neutron star is born it has a temperature of $\sim 10^{11}$ K but cools quickly via neutrino emission and spends most of its life at $\sim 10^6$ K (Heiselberg and Pandharipande 2000). Combining this temperature with the compactness of these objects (a typical radius is 10 km), we can estimate their total luminosity:

$$L_{\rm NS} \sim 4\pi(10 \text{ km})^2 \sigma(10^6 \text{ K})^4 \sim 10^{33} \text{ erg s}^{-1} \sim 1L_\odot. \tag{2}$$

Even though a neutron star can be as bright as the Sun, due to its high temperature its spectral energy distribution peaks at a much shorter wavelength than does that of the Sun. One may calculate this peak using Wien's displacement law:

$$\lambda_{\rm max} T \simeq 2.90 \times 10^{-3} \text{ m} \cdot \text{K} \tag{3}$$

which for a 10^6 K blackbody corresponds to $\lambda_{\rm max} \simeq 3$ nm, in the X-ray portion of the electromagnetic spectrum. The Earth's atmosphere is opaque to radiation at this energy, limiting neutron star detectors to space-based observatories. Since the first X-ray observatories were built only in the 1970s (*X-ray Astronomy* 2010) it is not surprising that the first detection of an isolated NS occured just 15 years ago.

In Fig. 1 is contained a current list of neutron star masses inferred from observations, organized by the type of binary star system in which the star was found.[1] The spread in mass shown in this figure is considerable, ranging from $0.7M_{\odot}$ to nearly $3M_{\odot}$. The average masses of each group are shown as vertical dotted lines, and error-weighted average masses are shown as vertical dashed lines. In each type of NS binary system both averages are close to $1.4M_{\odot}$. The most striking of these is J1748-2021B, a $\sim 2.8M_{\odot}$ NS, by a wide margin the most massive NS ever detected (Freire et al. 2008). In the following sections we will show how in the largest of these observed masses, with this object in particular, play a central role in constraining the nuclear EOS.

3 The Tolman-Oppenheimer-Volkoff (TOV) equation

Having reviewed the observational progress and difficulties of NSs we now turn to the mathematical construction of neutron star models. In 1939 R. C. Tolman, J. R. Oppenheimer and G. M. Volkoff solved the Einstein field equations for a perfect, self-gravitating, non-rotating, spherically symmetric, hydrostatic fluid (Oppenheimer and Volkoff 1939; Tolman 1939). The result, based on the interior Schwarzschild metric of the form

$$ds^2 = -e^{\Phi(r)}(cdt)^2 + \left(1 - \frac{2Gm(r)}{c^2 r}\right)^{-1} dr^2 + r^2(d\theta^2 + \sin^2\theta d\phi^2) \tag{4}$$

is an integro-differential equation for the pressure p which bears their names,

$$\frac{dp}{dr} = -\frac{Gm(r)\rho(r)}{r^2}\left(1 + \frac{p(r)}{\rho(r)c^2}\right)\left(1 + \frac{4\pi r^3 p(r)}{m(r)c^2}\right)\left(1 - \frac{2Gm(r)}{c^2 r}\right)^{-1} \tag{5}$$

(see Appendix for a derivation) where

$$m(r) \equiv \int_0^r 4\pi\rho(r')r'^2 dr', \tag{6}$$

and ρ is the mass-energy density:

$$\rho(T) \equiv \rho_0\left(1 + \frac{\epsilon(T)}{c^2}\right) \tag{7}$$

[1]Most of these NSs are in fact rotating pulsars. There exist analytic solutions to the Einstein equations for rotating spherical masses (see Kerr 1963) but calculations in this spacetime are *enormously* more complicated than those in non-rotating Schwarzschild spacetime and are beyond the scope of this discussion (see Hartle 1967). Fortunately for us, however, the effects of rotation on internal NS structure are insignificant except in objects with periods $\lesssim 1$ ms. (Heiselberg and Pandharipande 2000).

where ρ_0 is the rest mass, ϵ is the internal energy per baryon and T is the baryon temperature (Baumgarte and Shapiro 2010). The TOV solution also provides a differential equation for the metric component $\Phi(r)$:

$$\frac{d\Phi}{dr} = \frac{2Gm(r)}{c^2r^2}\left(1+\frac{4\pi r^3 p(r)}{m(r)c^2}\right)\left(1-\frac{2Gm(r)}{c^2r}\right)^{-1}. \tag{8}$$

There are some illuminating features of the TOV equation which deserve some attention. First, this equation is nothing more than the Newtonian differential equation of hydrostatic equilibrium with a few multiplicative correction terms. In the non-relativistic limit ($c \to \infty$) each of these corrections goes to unity. Second, each of the three correction terms is > 1, so relativistic effects always lead to a *steeper* pressure gradient in the star than in the Newtonian case. Third, in both the relativistic and non-relativistic cases, the RHS of the dp/dr equation is *negative* throughout the star; this means that $p(r)$ in every model decreases monotonically as r increases. (This last feature in particular is helpful in establishing boundaries on physically reasonable models, as we will discuss below.) Finally, the integrand in Eq. 6 is *not* simply ρdV for a spherically symmetric shell in this spacetime. To show this we recall that in general the 4-volume element dV is

$$dV = \sqrt{-g}d^4x \tag{9}$$

where $g \equiv \det g_{\alpha\beta}$, and $g_{\alpha\beta}$ is the metric tensor. For constant t (this is a hydrostatic model) the 3-volume element for a spherical shell in these coordinates is then

$$dV = 4\pi r^2(\sqrt{g_{rr}}dr) = 4\pi r^2\left(1-\frac{2Gm(r)}{c^2r}\right)^{-1/2} dr \tag{10}$$

For dV to remain finite, $r > 2Gm(r)/c^2$, in which case $dV(r) \geq 4\pi r^2 dr$. Therefore Eq. 6 will always be *smaller* than $\int \rho dV$. The negative contribution comes from the gravitational binding energy of the star.

One can transform the TOV integro-differential equation into two first-order differential equations by applying the Leibniz integral rule:

$$\frac{d}{dx}\left[\int_{f(x)}^{g(x)} h(x,y)dy\right] = \left(\frac{dg}{dx}\right)h(g,x) - \left(\frac{df}{dx}\right)h(f,x) + \int_{f(x)}^{g(x)}\frac{\partial}{\partial x}[h(x,y)]dy. \tag{11}$$

Applying this to $m(r)$, we have

$$\frac{dm}{dr} = 4\pi\rho(r)r^2. \tag{12}$$

We write $m(r)$ as an ODE rather than as an integral for simplicity in its numerical integration.

We then have three ordinary differential equations (5, 8 and 12) for four variables (p, ρ, m and Φ). To solve the system uniquely we require a fourth equation as well as three boundary conditions, one for each of the three first-order ODEs. However we note here that, in the course of solving the TOV system, we will neglect the solution for $\Phi(r)$. The reasons are twofold: first, because neither $p(r)$ nor $m(r)$ depend on $\Phi(r)$, one need not integrate it simultaneously with $p(r)$ and $\rho(r)$. Second, the physical interpretation of $\Phi(r)$ is of limited utility for our purposes in this paper; it describes the dilation or contraction of the coordinate time t and therefore contains information about the gravitational redshift of radiation emitted from the star, but the star's mechanical structure, with which we are chiefly concerned in this work, is unaffected by this quantity. In this case, we have only two ODEs (5 and 12) for three variables, p, ρ and m. We still require an equation relation p to ρ, as well as two boundary conditions for the two ODEs.

The EOS provides the link between p and ρ. To construct an EOS of the form $P = P(\rho, T)$ we turn to the first law of thermodynamics:

$$dU \equiv TdS - pdV + \sum_i \mu_i dN_i \tag{13}$$

where U is the total internal energy, S is the entropy, V is the fluid volume, μ_i and N_i are respectively the chemical potential and the number population of species i. A perfect fluid is isentropic so $dS = 0$, and its particle number is conserved so $dN = 0$. Then we have

$$dU = -pdV. \tag{14}$$

If we define U and V as the energy and volume *per baryon*, respectively, then we may write

$$V \equiv \frac{1}{n_b} \quad \rightarrow \quad dV = -\frac{1}{n_b^2} dn_b \tag{15}$$

where n_b is the baryon number density. From the definition of ρ,

$$dU = d(\rho c^2), \tag{16}$$

in which case

$$p = n_b^2 \frac{d(\rho c^2)}{dn_b} \tag{17}$$

Since $\rho = \rho(\rho_0, T)$, we now have $p = p(\rho_0, T)$ as desired. Most EOSs use Eq. 17, not Eq. 7 to calculate p.

There exists in the TOV equation no constraint on T; therefore to use a proper two-parameter EOS one must provide by some other means the complete temperature structure of the star. Fortunately even a poor guess for $T(r)$ should play a minor role in the overall structure of the star: in much of the NS the matter is at least as dense as nuclear matter ($n_{\rm nuc} \sim 0.16$ fm^{-3}), leading to Fermi energies of several 10 MeV (Heiselberg and Pandharipande 2000). The thermal contribution even at 10^6 K is only $kT \sim 100$ eV and is therefore negligible.

Despite the meager influence of thermal energy on the NS structure, a mere guess at T is undesirable. One solution is to exploit the isentropic nature of perfect fluids, in which case we may set T, p and ρ implicitly by forcing the EOS to follow an adiabat, along which the entropy S is constant. Alternatively, and more simply, we may assume the NS is isothermal and fix T everywhere. The latter is an especially popular choice; in fact, many workers simply set $T = 0$.

4 The Nuclear Equation of State

The nuclear EOS connects thermodynamic variables such as pressure, energy density and temperature, in a system composed of nuclear matter. It is of particular astrophysical interest because of its pivotal role in driving the dynamics of core-collapse supernova explosions, the result of which is the formation of neutron stars. However its precise nature continues to elude both the particle physics and astrophysics communities due to large uncertainties in the theory of the strong interaction, which is responsible for interactions among nucleons (Danielewicz 2001). A thorough study of the nuclear EOS requires a formidable command of quantum chromodynamics and a detailed discussion is beyond the scope of this work. Instead we examine in some detail a phenomenologically constructed EOS which contains both experimental and theoretical underpinnings, from Bethe and Johnson 1974 (BJ74).

4.1 The Liquid Drop Model

Many nuclear EOSs are based on an empirical model of the nucleus called the *liquid drop* model. (Incidentally the EOS we have chosen for calculations in this work is not, but the liquid drop model is popular enough that it nonetheless warrants a review here.) First suggested by G. Gamow, this model attempts to calculate the nuclear mass and binding energy using a number properties found in macroscopic liquid drops; in particular it assumes that the interior density is constant, and that the total binding energy of a nucleus is proportional to its mass (Martin 2009). C. F. von Weizsäcker quantified these and other properties through an equation called the *semi-empirical mass formula* (SEMF), which describes the total mass of the nucleus:

$$M(Z,A) = Z(M_p + m_e) + M_n(A-Z) - a_1 A + a_2 A^{2/3} \tag{18}$$

$$+ a_3 \frac{Z(Z-1)}{A^{1/3}} + a_4 \frac{\left(Z - \frac{A}{2}\right)^2}{A} + f_5(Z,A). \tag{19}$$

The first two terms represent the fermionic content of the nucleus: Z is the atomic number, A is the atomic weight, M_p is the proton mass, M_n is the neutron mass and m_e is the electron mass.

The next five terms contain correction factors, with $a_i > 0$. The third term on the RHS, $-a_1 A$, is a volume correction term, which accounts for the saturation of the strong force, causing only neighboring nucleons to interact with one another via gluon exchange. (The Coulomb and gravitational forces, in contrast, exhibit no such saturation.) Experimental evidence shows that the nuclear radius goes like $A^{1/3}$, so the volume, or mass, goes like $(A^{1/3})^3 = A$. It is the only of the five correction terms in the SEMF which contributes to the binding energy and *reduces* the nuclear mass. The fourth term, $a_2 A^{2/3}$, accounts for an overestimation in the volume correction term, since nucleons on the surface of the nucleus are not surrounded. The term is proportional to the surface area, which goes like the square of the radius, or $(A^{1/3})^2 = A^{2/3}$. The next term, $a_3 \frac{Z(Z-1)}{A^{1/3}}$, represents the Coulomb interactions among the protons in the nucleus. The penultimate term, $a_4 \frac{(Z-A/2)^2}{A}$, accounts for the tendency of nuclei to have equal numbers of protons and neutrons. The last term is a *pairing term*,

$$f_5(Z,A) = \begin{cases} -a_5 A^{-1/2} & \text{if } Z, N \text{ even} \\ +a_5 A^{-1/2} & \text{if } Z, N \text{ odd} \\ 0 & \text{otherwise} \end{cases} \tag{20}$$

which describes the tendency of like nucleons in the same spatial state to couple, producing an overall spin-0 state (Martin 2009).

4.2 Bethe and Johnson (BJ74)

Rather than fitting mass and simple binding energy formulae to experimental data as most SEMF-based EOSs do, BJ74 instead calculates nucleon-nucleon interactions directly using non-relativistic, many-body theory. The strong force is modeled empirically by accounting for its attraction between distant nucleons and repulsion between nearby nucleons. Physically they assume the long-distance attractive component is due to exchange of scalar mesons (that is, spin-0 mesons with even parity), while the short-range repulsive core is due to exchange of vector mesons (spin-1 mesons with odd parity); mathematically they represent this interaction using a *Reid core* potential (Reid 1968), which consists of attractive and repulsive Yukawa potentials:

$$V_{AB} = (\mu r)^{-1} \sum_n C_n(AB) e^{-n\mu r} \tag{21}$$

where the C_n are positive or negative coefficients whose values depend on the interacting nucleons A and B as well as the angular momenta of each, and $\mu \equiv mc/\hbar$ is the reciprocal Compton wavelength of the meson (with mass m) exchanged between the two nucleons. It is these coefficients, rather than those discussed in the previous subsection, which are fitted to experimental results, specifically phase shifts in nucleon scattering. BJ74 modify slightly the Reid core, in that while Reid required $n \in \mathbb{Z}$, BJ74 allow $n \in \mathbb{R}$. There are many more details in this EOS than are presented here, and we refer the interested reader to Bethe and Johnson 1974.

5 TOV's Role in Compact Object Astrophysics

One noteworthy feature of self-gravitating compact objects such as NSs is the existence of a finite maximum mass. That is, for a given nuclear EOS there exists a single central density ρ_c which produces the most massive star possible in stable mechanical equilibrium. Stars with lower masses than this are also stable, but those above are not and therefore do not exist in nature. In neutron stars this mass is called the *TOV mass* or the *TOV limit*, which in 1939 Tolman, Oppenheimer and Volkoff calculated to be about $0.7M_\odot$. As will be shown below, this value is much lower than predictions with current models. The reason is that the authors assumed the NS is composed of a completely degenerate, non-interacting neutron gas, the EOS for which is extremely "soft," meaning a small change in P causes a large change in ρ.

Astronomers and particle physicists alike place such faith in the predictions of general relativity that one of their primary methods of constraining the nuclear EOS (which remains largely unknown) consists of observing neutron star masses and comparing them with the largest masses predicted by various EOSs (Lattimer and Prakash 2005; Lattimer 2007). That two branches of physics conspire across so many orders of magnitude in scale to answer a single scientific query illustrates a truly remarkable property of the TOV model.

6 Numerical Methods

The TOV differential equations for p and m are coupled and therefore must be integrated simultaneously; the equation for Φ, however, is decoupled and can be solved after $p(r)$ and $m(r)$ have been found, although we will not do so in this work. The P and ρ ODEs are well behaved (non-singular, non-oscillatory, etc.) in the domain $r > 0$ and $p > 0$ and therefore may be integrated using even very simple numerical methods.

We have written a code[2] in `C` called `TOV_solver` which integrates the TOV equations using the fifth-order Runge-Kutta Dormand-Prince algorithm (Dormand and Prince 1980). The code calls the EOS in a modular way such that the user may use any EOS he wishes. Alternatively, if an EOS cannot easily be incorporated into the code, or if its source code is not publically available, `TOV_solver` can interpolate thermodynamic data from tables. Most public EOSs such as Ishizuka et al. 2008, Cooperstein 1985 and Timmes and Swesty 2000 are written in "callable" form, in anticipation of being used in a wide variety of simulation codes. `TOV_solver` exploits this fact and consequently may be used to constrain the nuclear EOS by comparing their maximum predicted masses of neutron stars with those masses inferred from observation.

Before we can integrate the TOV equations we must specify boundary conditions. First, as discussed at length in Oppenheimer and Volkoff 1939 the only value of $m(r = 0) \equiv m_c$ which prevents the metric tensor component g_{rr} from diverging is $m_c = 0$. Also, we define the surface of the star as the location R where $p(r = R) = 0$. The only free parameter in this system of equations is therefore $\rho(r = 0) \equiv \rho_c$. Setting this value manually allows us to integrate the TOV equation and calculate the complete mechanical structure of the star, including its total mass $m(r = R) \equiv M$.

7 Analysis of Results

7.1 Thermodynamic Predictions of BJ74

Before showing any NS calculations we first show some of the characteristic thermodynamic properties of BJ74 in Fig. 2. In this plot and throughout this work we have used $T = 0$,

[2]The source is freely available at GitHub: `http://git.io/QUGTIg`.

owing to the insignificance of thermal effects. In the majority of this plot the EOS follows a nearly straight line in the log-log plot, corresponding to a power-law relationship, the value of the power being equal to the slope of the line. It is for this reason that polytropic (power-law) representations of EOSs, which have the form $p \sim \rho^\Gamma$, remain so popular.

7.2 Internal NS Structure

We now explore the structure of a typical NS through the relations $p(r)$, $m(r)$ and $\rho(r)$ for a given EOS and ρ_0. However we must first address a complication which plagues all calculations performed in GR, namely that the curvature of spacetime changes the physical representation of the coordinates chosen for the calculation. In this case the problem lies in that the proper length ds as defined in Eq. 4 is not linear in the coordinate dr. In flat spacetime we could write the metric as

$$ds^2 = -(cdt)^2 + dr^2 + r^2(d\theta^2 + \sin^2\theta d\phi^2) \tag{22}$$

in which case one could treat r exactly as in a solid, Euclidean 2-sphere: at a given fixed time t it is a coordinate whose value is zero at the center of the sphere, reaches a maximum at the sphere's surface, and increases linearly along a geodesic connecting those two points.

In the interior Schwarzschild spacetime, however, this is no longer the case, and we must scrutinize the "radial curvature" in order to determine if we can perform at least a qualitatively accurate analysis of the NS using r as a radius. (In the exterior Schwarzschild solution the radial coordinate r diverges as one approaches the Schwarzschild radius, even though the spacetime at that point is physically well-behaved.) One way to do this is to calculate the Riemann tensor $R_{\alpha\beta\gamma\delta}$, the Ricci tensor $R_{\alpha\beta}$ or the curvature scalar R as a function of r. However we choose a slightly more intuitive approach: we calculate the structure of a NS with $\rho_0 = 10^{15}$ g cm^{-3} using BJ74, and in Fig. 3 we plot the quantity ds/dr, which is just $(1 - 2Gm(r)/c^2r)^{-1/2}$, versus r. A value of unity in this figure indicates flat spacetime. If the space were flat or nearly so, we could perform this calculation using the much simpler Newtonian formulation of gravity. We see in the figure that deviations from unity are significant, with $|(dL/dr) - 1| \lesssim 25\%$. If we ignored relativistic effects these deviations would most likely result in errors of this magnitude or more in the prediction of the TOV limit. However the interior coordinate r diverges nowhere within the star, and so in the following qualitative discussions we will treat it as a radius in a Euclidean 2-sphere.

We are now equipped to study the mechanical structure of a typical NS. Again using the BJ74 EOS with $\rho_0 = 10^{15}$ g cm^{-3}, we show $m(r)$ and $\rho(r)$ in Figs. 4 and 5, respectively. Both figures show that the BJ74 result corroborates the canonical NS model which consists of a super-dense body with a very thin "atmosphere." The low-density region (in Fig. 4 the region where m(r) is flat) is very narrow and in Fig. 5 ρ stays nearly constant from the core all the way to the surface, then drops to zero in a span of $\Delta r \lesssim 1$ km.

We note also that the region of maximum spacetime curvature is at $r \sim 10$ km in Fig. 3. This corresponds to the location of the majority of the stellar mass as shown in Fig. 4. This verifies the intuitive interpretation of the theory of general relativity: more mass (energy) leads to more curvature.

7.3 The TOV Limit

Among the most popular calculations performed with the TOV equations with a particular EOS are the mass-radius and mass-central density relations. Pictoral summaries of current progress in this field are shown in Fig. 6 (mass-radius) and in Fig. 7 (mass-central density). These figures show a wide distribution of maximum mass predictions, ranging from 1.3 $M_\odot$ to 2.8 $M_\odot$. One is able to validate (or invalidate) an EOS by calculating the TOV limit and searching for any observed non-rotating NS masses which are larger. If such stars exist, then the EOS must be incorrect or incomplete.

The number of observed NS stars with inferred masses is small, and until a much larger sample is compiled, and the observational uncertainties reduced, one cannot use them confidently to rule out any EOS. However the results compiled so far are nevertheless quite informative. We draw special attention to the pulsar J1748-2021B in Fig. 1, whose mass of $2.8M_\odot$ (with small error bars) is so far the largest of any observed NS. It is also larger than the TOV limit of nearly every EOS in Figs. 6 and 7. The discovery of this pulsar, if its inferred mass is correct, will have profound effects on the study of the nuclear EOS, since nearly every one is too soft to attain a mass so large.

In Fig. 8 we show the mass-central density relation for BJ74, and in Fig. 9 we show the mass-radius relation. BJ74 predicts a maximum NS mass of $\sim 1.9M_\odot$, which is slightly lower than the average of the EOSs show in Fig. 6, but toward the upper end of the observed masses in Fig. 1. Not only is its maximum mass prediction close to those of other EOSs, but also does the overall shape of its mass-radius and mass-central density relations. However, like the other EOSs, its TOV limit falls well below the $2.8M_\odot$ of the pulsar J1748-2021B.

8 Summary

We have developed the mathematical framework to calculate the complete mechanical structure of a spherically symmetric, non-rotating, static mass composed of a perfect fluid in general relativity. Within this framework we have included a modern nuclear EOS, BJ74, in order to calculate the maximum mass of a non-rotating neutron star. This EOS predicts $\sim 1.9M_\odot$, in rough agreement with other EOSs. We have also compared this result to a list of observed NS masses and found it be larger than most. However BJ74 and almost every other nuclear EOS appear to conflict with a recently discovered $2.8M_\odot$ pulsar which, if the mass estimate of this object is accurate, indicates that there exists some crucial nuclear processes which have yet to be discovered.

References

Baumgarte, Thomas W. and Stuart L. Shapiro (2010). *Numerical Relativity: Solving Einstein's Equations on the Computer*. Cambridge, UK: Cambridge University Press.

Bethe, H.A. and M.B. Johnson (1974). “Dense baryon matter calculations with realistic potentials.” In: *Nuclear Physics A* 230.1, pp. 1 –58. ISSN: 0375-9474. DOI: 10.1016/0375-9474(74)90528-4. URL: http://www.sciencedirect.com/science/article/pii/0375947474905284.

Chen, K. and M. Ruderman (Jan. 1993). “Pulsar death lines and death valley.” In: *Astrophysical Journal* 402, pp. 264–270. DOI: 10.1086/172129.

Cooperstein, J. (1985). In: *Nucl. Phys.* A438, p. 722.

Danielewicz, Paweł (2001). “Nuclear equation of state.” In: *AIP Conference Proceedings* 597.1. Ed. by Xizhen Wu et al., pp. 24–42. DOI: 10.1063/1.1427443. URL: http://link.aip.org/link/?APC/597/24/1.

Dormand, J.R. and P.J. Prince (1980). “A family of embedded Runge-Kutta formulae.” In: *Journal of Computational and Applied Mathematics* 6.1, pp. 19 –26. ISSN: 0377-0427. DOI: 10.1016/0771-050X(80)90013-3. URL: http://www.sciencedirect.com/science/article/pii/0771050X80900133.

Freire, P. C. C. et al. (Mar. 2008). “Eight New Millisecond Pulsars in NGC 6440 and NGC 6441.” In: *Astrophysical Journal* 675, pp. 670–682. DOI: 10.1086/526338. arXiv:0711.0925.

Hartle, J. B. (Dec. 1967). “Slowly Rotating Relativistic Stars. I. Equations of Structure.” In: *Astrophysical Journal* 150, p. 1005. DOI: 10.1086/149400.

Heiselberg, Henning and Vijay Pandharipande (2000). “RECENT PROGRESS IN NEUTRON STAR THEORY.” In: *Annual Review of Nuclear and Particle Science* 50.1, pp. 481–524. DOI: 10.1146/annurev.nucl.50.1.481. eprint: http://www.annualreviews.org/doi/pdf/10.1146/annurev.nucl.50.1.481. URL: http://www.annualreviews.org/doi/abs/10.1146/annurev.nucl.50.1.481.

Hewish, A. et al. (Feb. 1968). “Observation of a Rapidly Pulsating Radio Source.” In: *Nature* 217, pp. 709–713. DOI: 10.1038/217709a0.

Hughston, L. P. and K. P. Tod (1990). *An Introduction to General Relativity*. Cambridge, UK: Cambridge University Press.

Ishizuka, C. et al. (Aug. 2008). “Tables of hyperonic matter equation of state for core-collapse supernovae.” In: *Journal of Physics G Nuclear Physics* 35.8, p. 085201. DOI: 10.1088/0954-3899/35/8/085201. arXiv:0802.2318 [nucl-th].

Kerr, Roy P. (1963). “Gravitational Field of a Spinning Mass as an Example of Algebraically Special Metrics.” In: *Phys. Rev. Lett.* 11 (5), pp. 237–238. DOI: 10.1103/PhysRevLett.11.237. URL: http://link.aps.org/doi/10.1103/PhysRevLett.11.237.

Lattimer, J. M. and M. Prakash (2001). “Neutron Star Structure and the Equation of State.” In: *The Astrophysical Journal* 550.1, p. 426. URL: http://stacks.iop.org/0004-637X/550/i=1/a=426.

Lattimer, J. M. and M. Prakash (Mar. 2005). “Ultimate Energy Density of Observable Cold Baryonic Matter.” In: *Physical Review Letters* 94.11, 111101, p. 111101. DOI: 10.1103/PhysRevLett.94.111101. eprint: arXiv:astro-ph/0411280.

Lattimer, James (2007). “Equation of state constraints from neutron stars.” In: *Astrophysics and Space Science* 308 (1). 10.1007/s10509-007-9381-3, pp. 371–379. ISSN: 0004-640X. URL: http://dx.doi.org/10.1007/s10509-007-9381-3.

Martin, B. R. (2009). *Nuclear and Particle Physics*. 2nd. Chichester, West Sussex, UK: John Wiley & Sons Ltd.

Oppenheimer, J. R. and G. M. Volkoff (Feb. 1939). “On Massive Neutron Cores.” In: *Physical Review* 55, pp. 374–381. DOI: 10.1103/PhysRev.55.374.

Reid, Roderick V. (1968). “Local phenomenological nucleon-nucleon potentials.” In: *Annals of Physics* 50.3, pp. 411 –448. ISSN: 0003-4916. DOI: 10.1016/0003-4916(68)90126-7. URL: http://www.sciencedirect.com/science/article/pii/0003491668901267.

Timmes, F. X. and F. D. Swesty (Feb. 2000). “The Accuracy, Consistency, and Speed of an Electron-Positron Equation of State Based on Table Interpolation of the Helmholtz Free Energy.” In: *Astrophysical Journal Supplement* 126, pp. 501–516.

Timmes, Frank X. (Nov. 2011). *Cold Neutron Stars*. URL: http://cococubed.asu.edu/images/nstar/rho_mass_web_large.jpg.

Tolman, R. C. (Feb. 1939). “Static Solutions of Einstein’s Field Equations for Spheres of Fluid.” In: *Physical Review* 55, pp. 364–373. DOI: 10.1103/PhysRev.55.364.

Walter, F. M., S. J. Wolk, and R. Neuhäuser (Jan. 1996). “Discovery of a nearby isolated neutron star.” In: *Nature* 379, pp. 233–235. DOI: 10.1038/379233a0.

X-ray Astronomy (Dec. 2010). URL: http://imagine.gsfc.nasa.gov/docs/science/know_l2/history_xray.html.

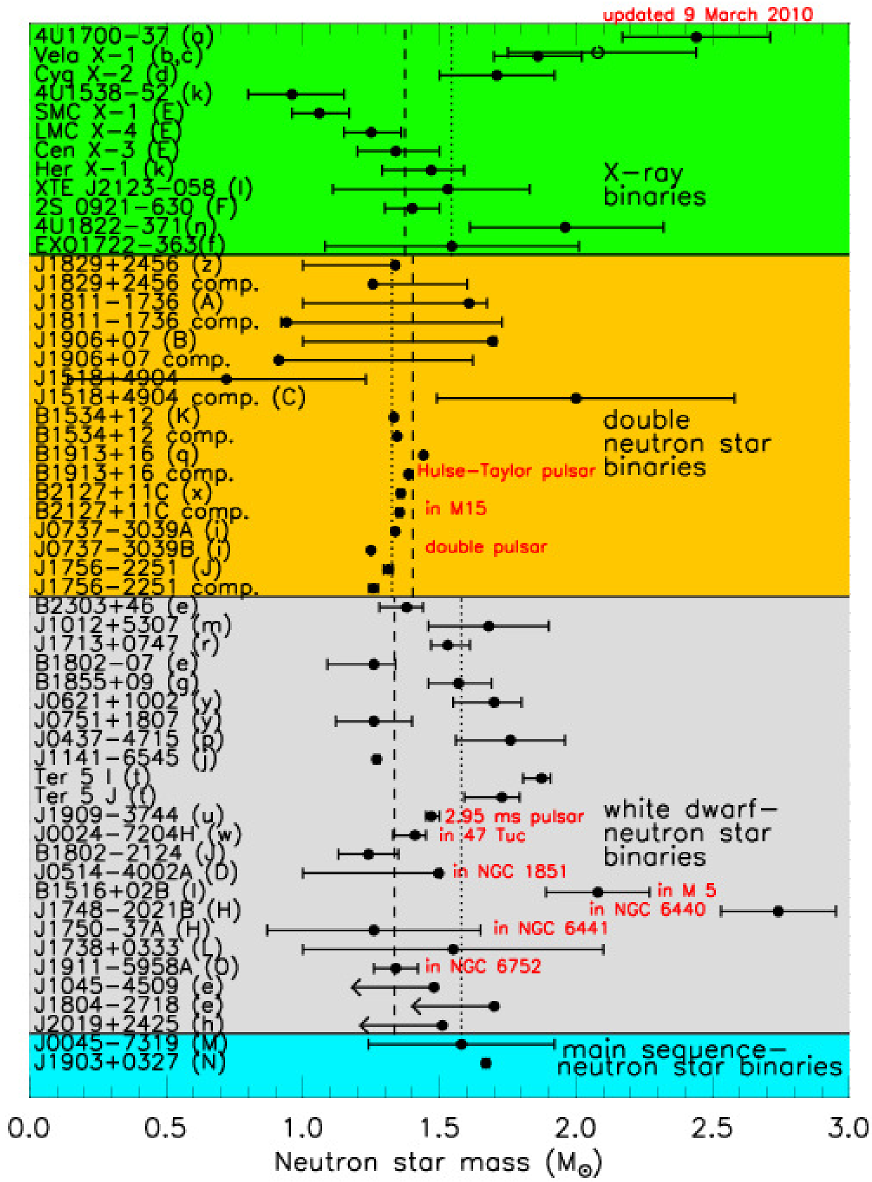

Figure 1: A list of neutron star masses inferred from observations of binary systems. The vertical dotted lines indicate the average masses in each type of system; the dashed lines are error-weighted averages. This figure is an updated version of Fig. 2 of Lattimer and Prakash 2005.

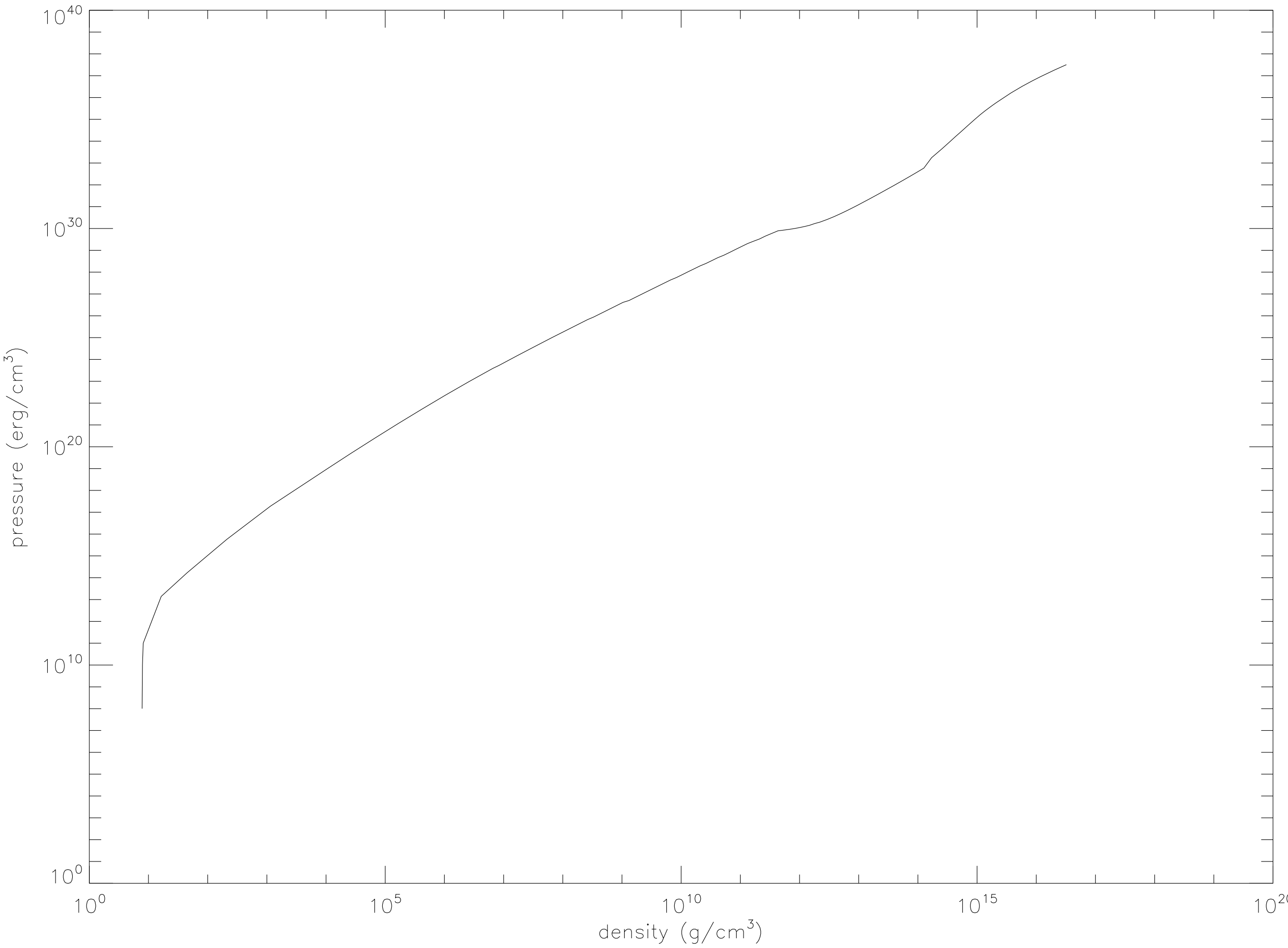

Figure 2: Pressure vs. density for BJ74 at $T = 0$ K.

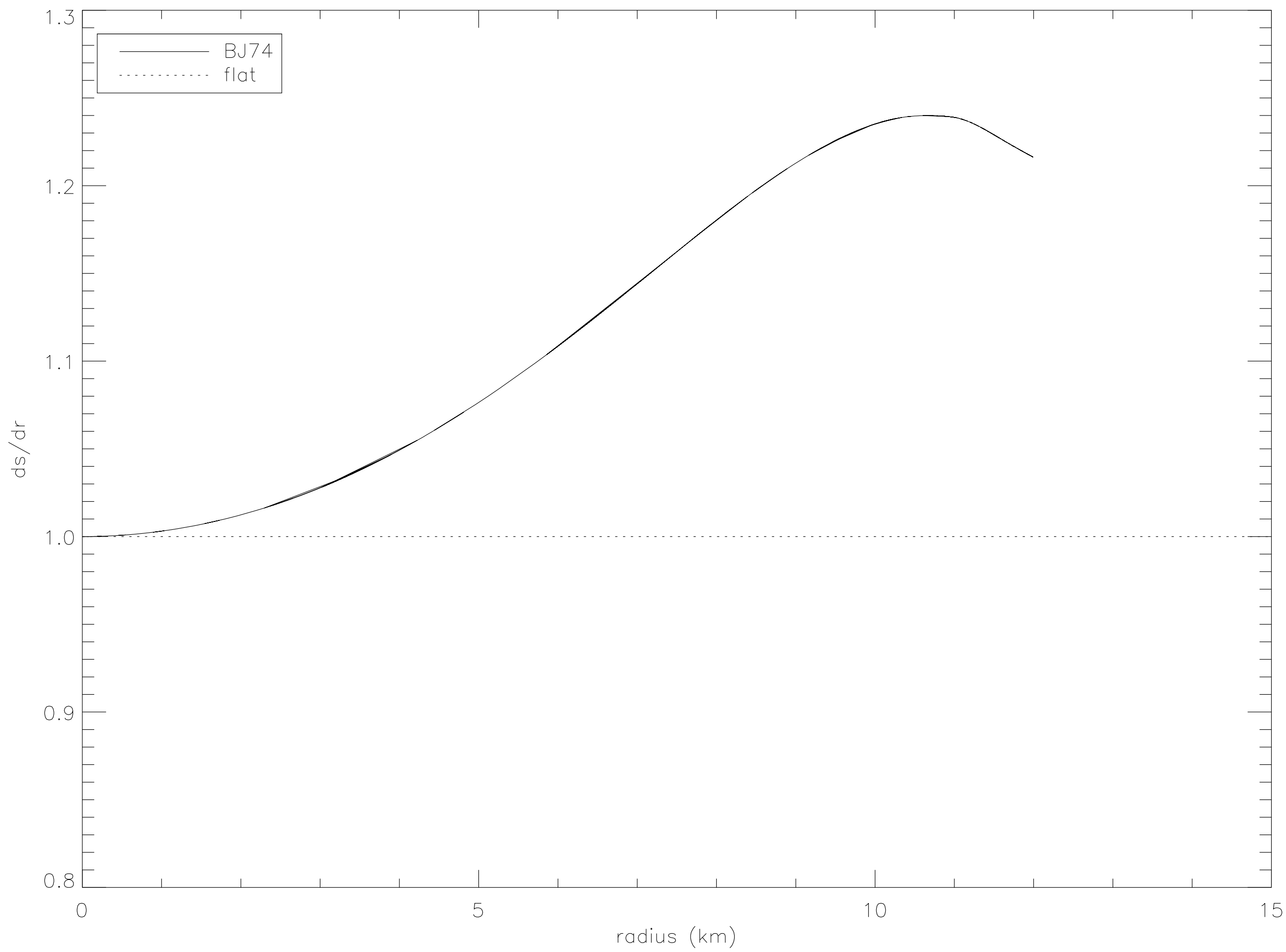

Figure 3: Comparison of geodesic length ds with "radial" coordinate length dr for a NS using BJ74 with a central density of $\rho_0 = 10^{15}$ g cm^{-3} (solid line). A value of $ds/dr = 1$, shown as the dotted line, indicates s is linear in r, i.e., the spacetime is flat along the radial direction. The NS spacetime deviates up to 25% from the flat spacetime result, showing that neglecting GR effects could results in errors of this magnitude or larger.

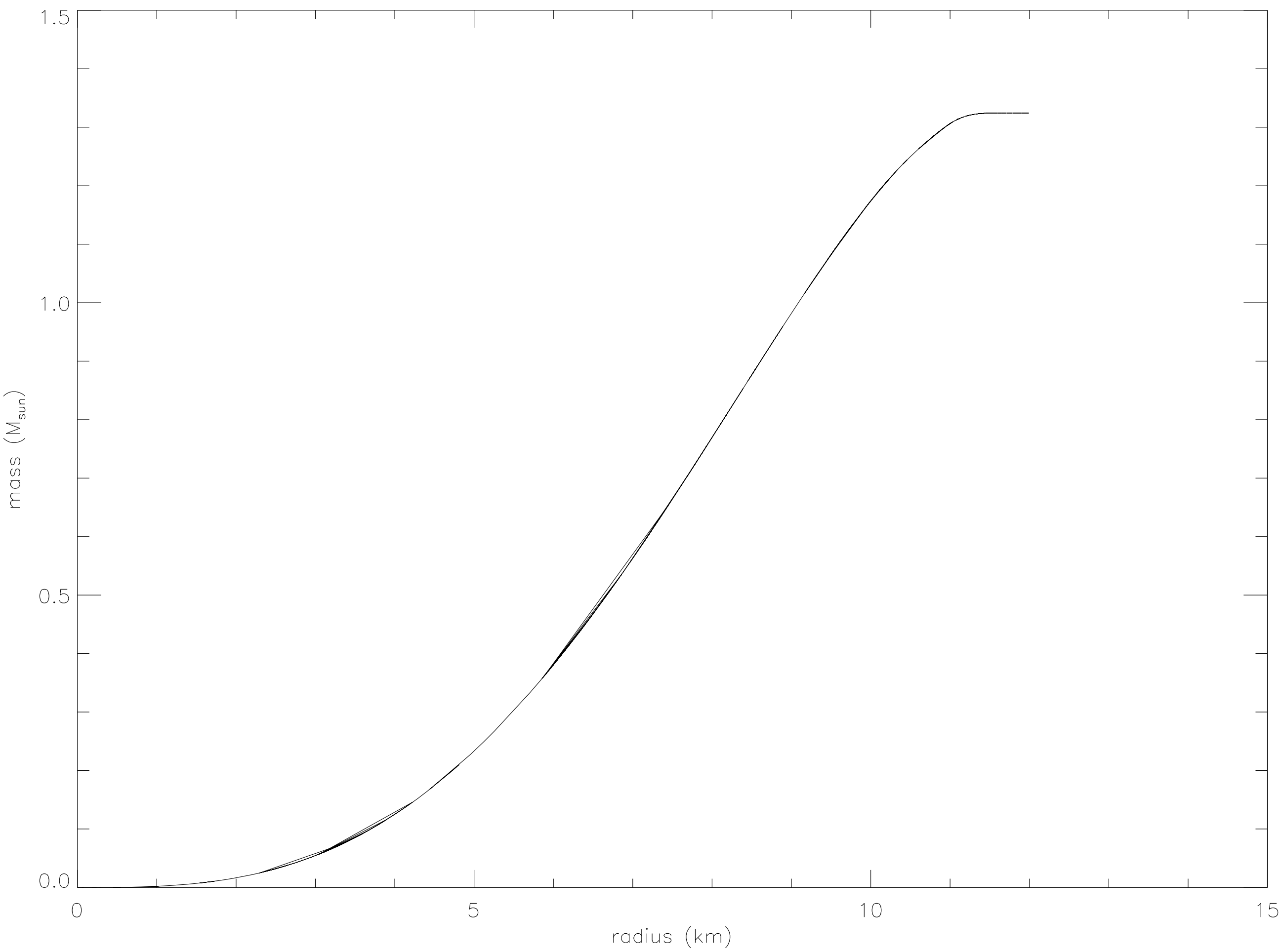

Figure 4: Inclusive mass vs. radius for a NS using BJ74 with $\rho_0 = 10^{15}$ g cm^{-3}.

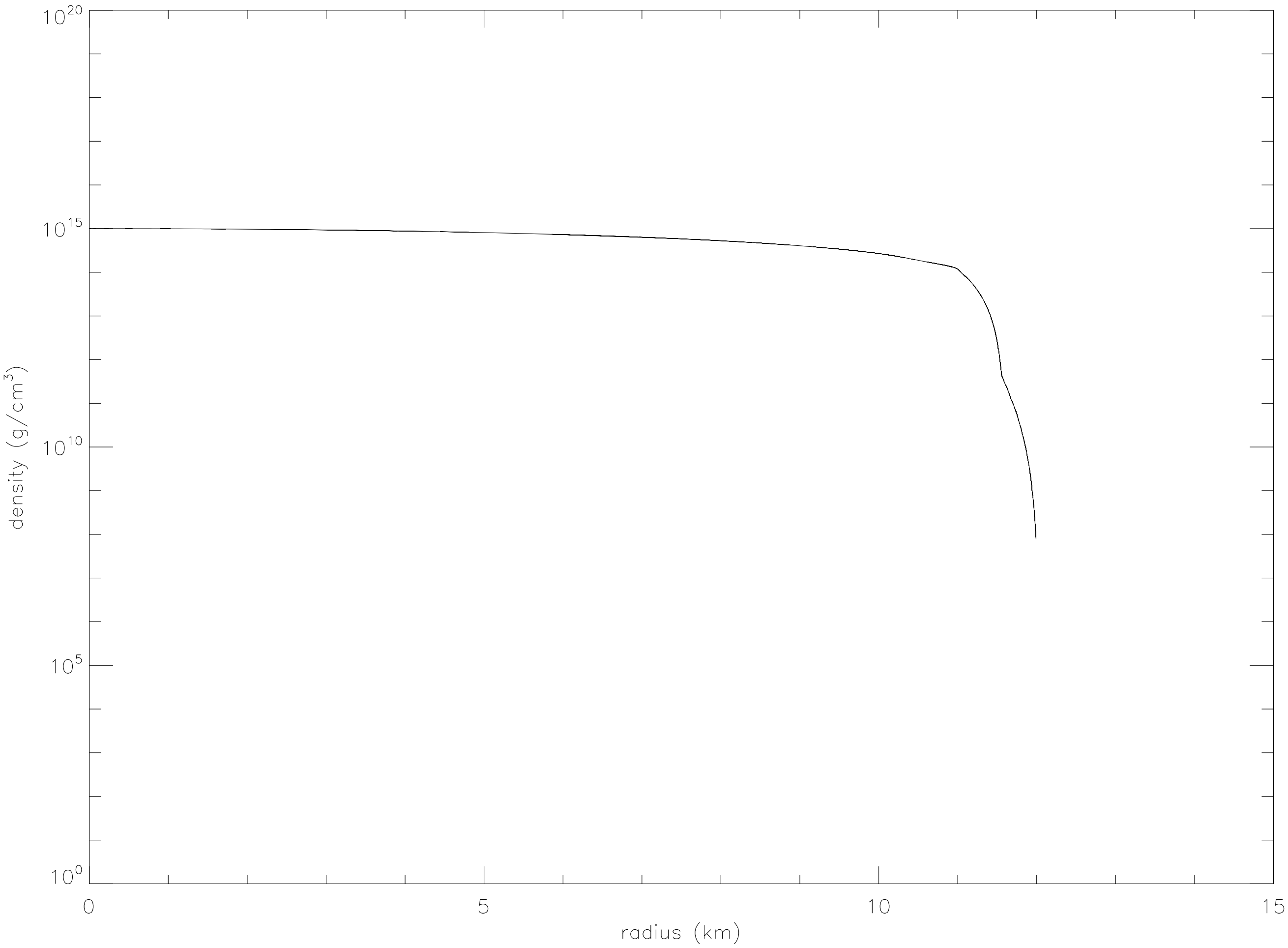

Figure 5: Mass density vs. radius for a NS using BJ74 with $\rho_0 = 10^{15}$ g cm^{-3}.

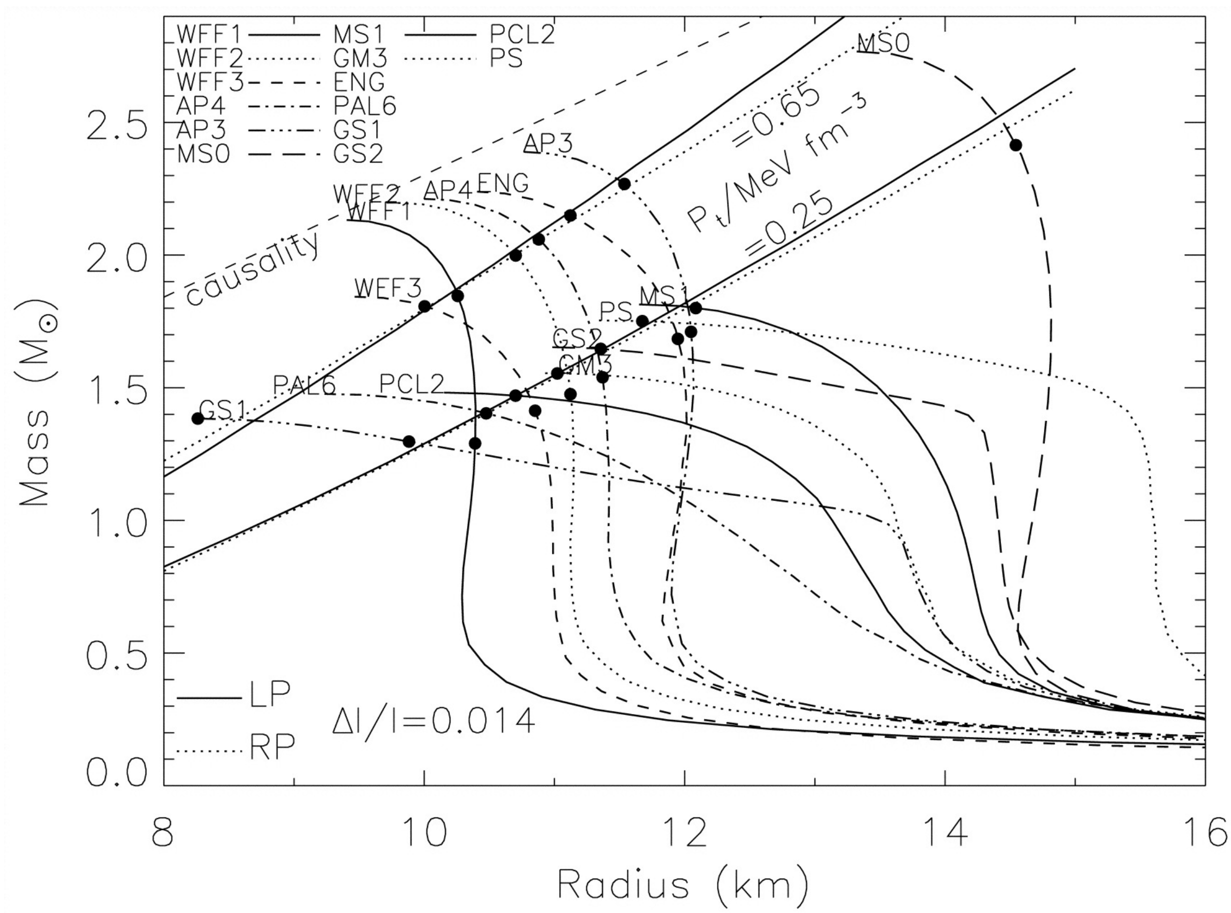

Figure 6: Mass-radius relation for neutron stars according to different nuclear EOSs. This figure is Fig. 7 of Lattimer and Prakash 2001. The predicted maximum masses as well as their corresponding radii are quite disparate.

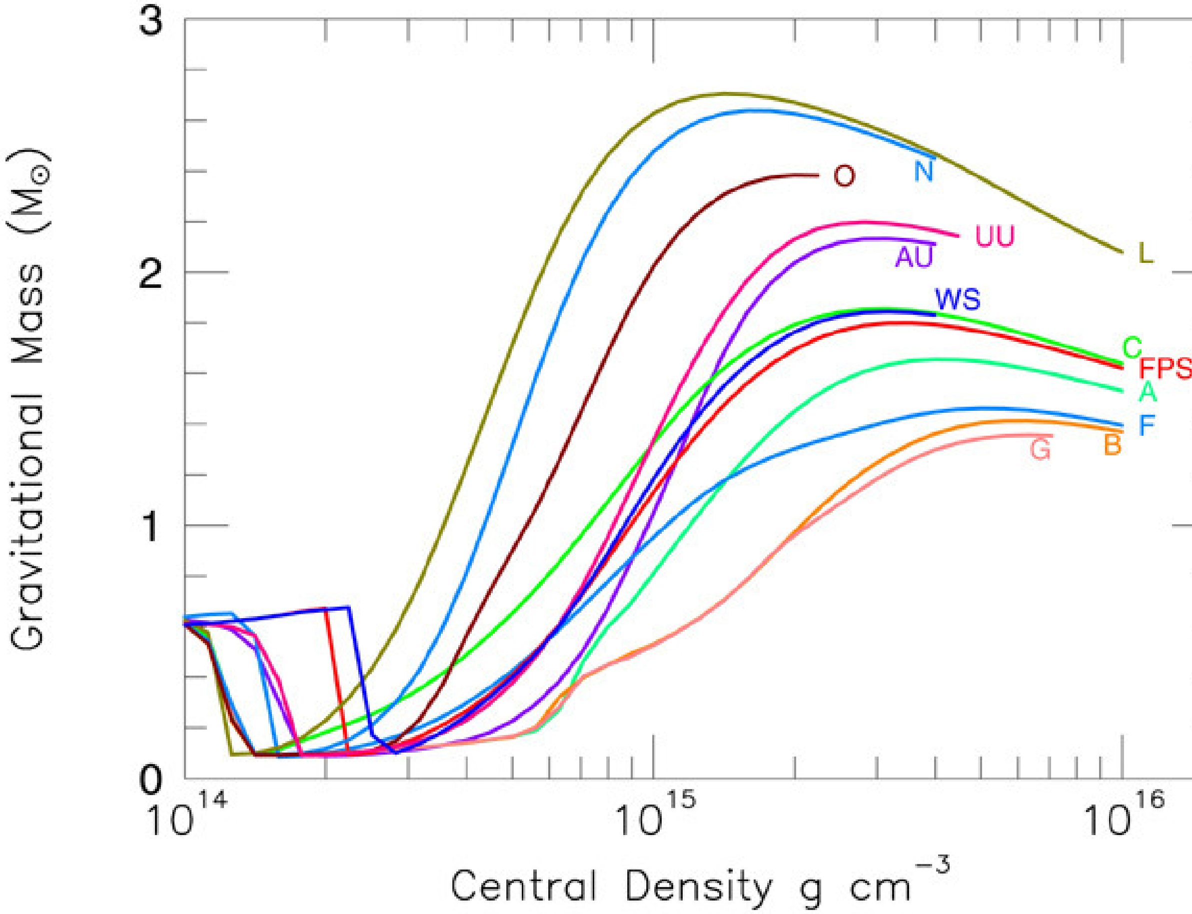

Figure 7: Mass-central density relation for neutron stars with different EOSs. Taken from Timmes 2011.

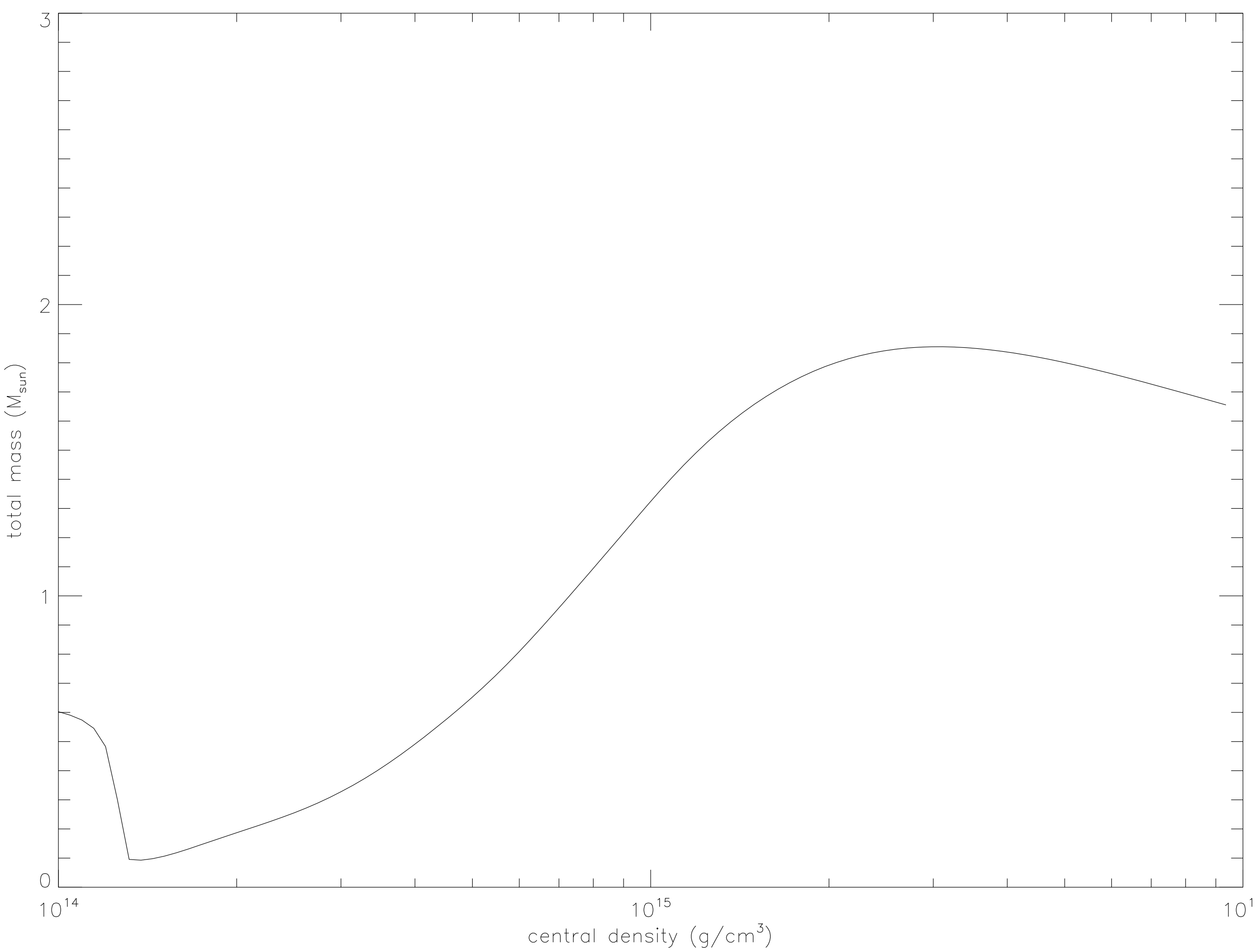

Figure 8: Mass-central density relation predicted by BJ74.

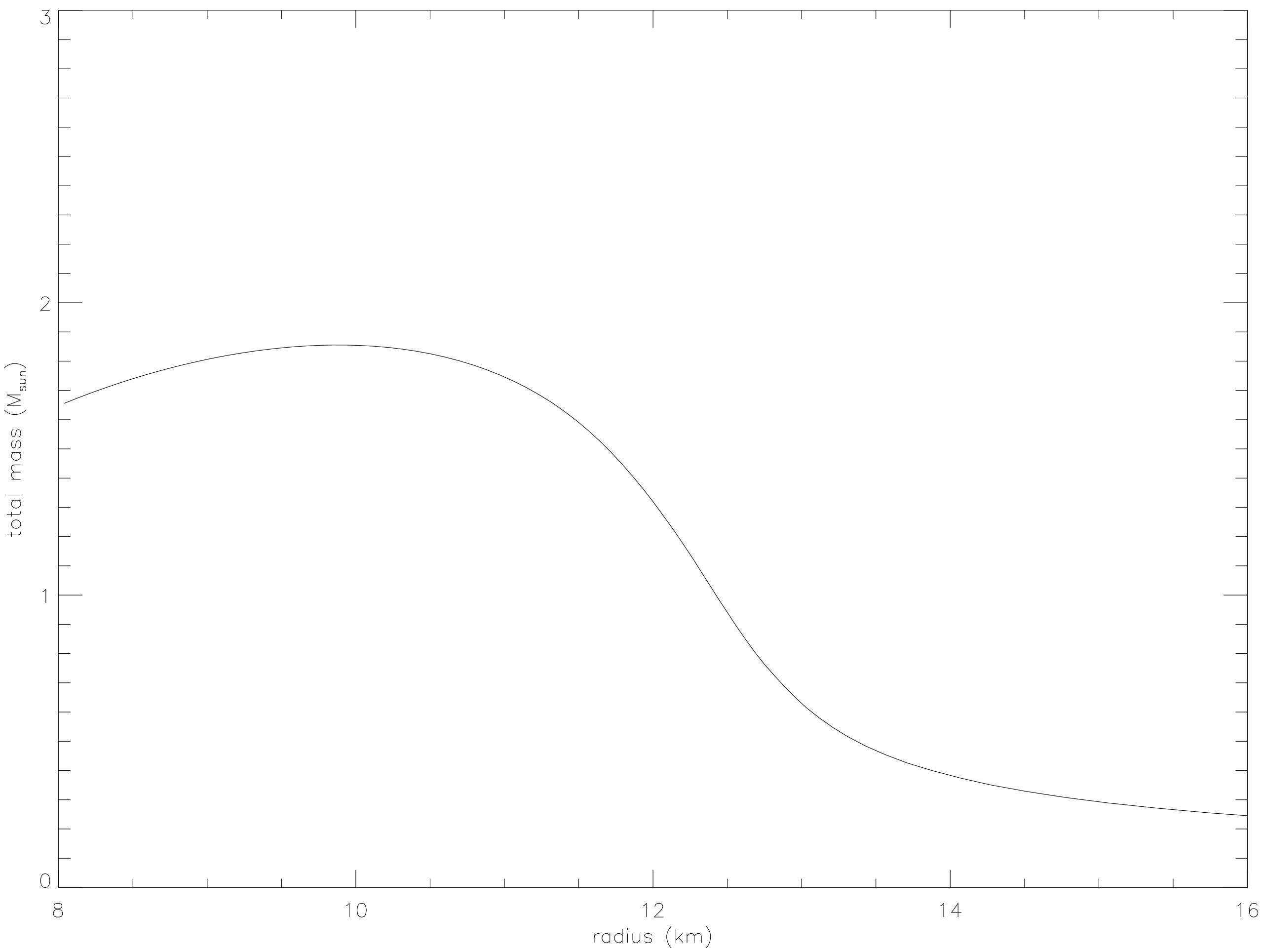

Figure 9: Mass-radius relation predicted by BJ74.